

Seasonal variability of wind and thermohaline-driven circulation in the Black Sea: Modeling studies

Temel Oguz

Institute of Marine Sciences, Middle East Technical University, Erdemli, Icel, Turkey

Paola Malanotte-Rizzoli

Department of Earth, Atmospheric and Planetary Sciences, Massachusetts Institute of Technology, Cambridge

Abstract. The seasonal variability of the Black Sea circulation is studied using an eddy-resolving primitive equation model. A series of numerical experiments is carried out to determine the relative importance of wind stress, air-sea thermohaline fluxes, and river-induced lateral buoyancy forcing in driving the circulation on the monthly and seasonal timescales. A synthesis is made of the results with those obtained under yearly climatological conditions by *Oguz et al.* [1995] to assess whether the major circulation features are a response to the yearly forcings or are dominated by the seasonal cycle. The model experiments indicate that under all forcing mechanisms, the overall basin circulation is characterized by a very strong seasonal cycle dominating the yearly signal described by *Oguz et al.* [1995]. The purely wind-driven circulation reveals most of the observed circulation features including a well-defined meandering boundary current system and subbasin scale cyclonic gyres forming the interior flow structure of the basin. Topography obviously remains a crucial factor in controlling the pattern of the persistent rim current system all year long. The dynamical instabilities of the rim current produce strong meandering and mesoscale eddies which often modulate the basin and subbasin scale structures of the circulation. The surface thermohaline fluxes generate simpler circulation patterns with a comparable strength but mostly in the opposite direction to the wind-driven circulation. Two important by-products emerge from the present work. First is the necessity of reanalyzing the heat flux climatology. The existing surface thermohaline fluxes, even though not affecting critically the general characteristics of the surface circulation patterns, may induce rather unrealistic horizontal temperature distributions and water mass properties in the surface layer. Second, the role of the northwestern shelf in the cold intermediate water (CIW) mass formation process is shown to be secondary during moderate-to-high winter discharge conditions from the northwestern rivers. In these conditions the freshwater outflow reduces the density of the cold water formed on the shelf by about 1 kg/m^3 as compared with that of the basin interior, which is the major reservoir for the formation of the winter CIW.

1. Introduction

Intense observational and computational efforts have recently been devoted to exploring the oceanographic characteristics of this relatively unknown, and in many respects, challenging sea. Numerous regional studies were performed by oceanographic institutions of the riparian countries through their national programs. The basin as a whole, however, has been investigated thoroughly only after the late 1980s within the framework of several international and/or multiinstitutional programs. The basin-wide multiship surveys, performed on a medium-resolution station network with approximately 20-nm spacing, have provided several quasi-synoptic realizations of the circulation and of the water mass characteristics. The picture of the upper layer circulation that emerged from the pooled data sets as well as from satellite imagery is a step forward to the existing classical view. It involves multiple scales of motion ranging from subbasin gyres to mesoscale eddies.

The peripheral current system is identified as a highly variable entity with intense meanders, offshore jets, and ring formation events. The interior circulation shows a pattern of interconnected cyclonic gyres with typical dimensions of $\sim 100 \text{ km}$, interacting together as well as with the rim current system. Many features of the circulation, however, must still be explored. The relative contributions of major driving forces and the roles of internal dynamical processes to the circulation in different seasons are still not clear.

The Black Sea may be considered as one of the best examples of marginal seas of the world oceans. It is a nearly enclosed basin having a limited exchange with the Mediterranean through a narrow passage ($\sim 1 \text{ km}$) of the Bosphorus Strait. It is a dilution basin in which the excess of net freshwater input (river discharges and precipitation) over evaporation is balanced by the net outflow of $\sim 300 \text{ km}^3/\text{yr}$ from the sea through the Bosphorus. The basin circulation is affected by all major driving mechanisms (wind, surface heat and salt fluxes, lateral buoyancy fluxes). The wind stress curl generates a persistently cyclonic circulation in the basin. This tendency is, on one hand, reinforced by the coastal freshwater-driven component of the

Copyright 1996 by the American Geophysical Union.

Paper number 96JC01093.
0148-0227/96/96JC-01093\$09.00

circulation and, on the other hand, may be frequently disrupted by the thermohaline circulation induced by uneven cooling and/or warming of the basin. As shown by *Oguz et al.* [1995], the horizontal structure of the circulation within the upper layer of approximately 100-m depth depends crucially on the relative strength of the wind stress and the surface flux forcings. For the climatological data used in the above study, horizontal variability of the annual mean heat flux modifies the cyclonic basin-wide wind-driven circulation by producing a major anticyclonic gyre in the southwestern part of the sea.

Numerical modeling efforts performed within the last 2 decades have been reviewed earlier by *Oguz et al.* [1995] and will not be repeated here. Presently, there are a series of ongoing parallel efforts on different aspects of the Black Sea general circulation problem. *Oguz et al.* [1995] studied the wind and thermohaline circulation driven by the yearly mean climatological forcings. *Stanev et al.* [1995] deal with the high-frequency variability of the circulation in response to half a daily atmospheric forcing. S. P. Meacham (On the circulation of the Black Sea at the basin scale and the mesoscale, submitted to *Journal of Geophysical Research*, 1996) investigates the basin scale and mesoscale interactions and evolution of mesoscale structures developing from the instabilities of the rim current.

In the present study we pursue our efforts to define the relative contributions of different forcings in driving the seasonal circulation patterns. Using a systematic series of experiments, our aim is to explore the possible role of each independent forcing in generating major features of the circulation. Combining the findings of this study with the previous one given by *Oguz et al.* [1995], we then wish to identify the seasonal and year-round persistent features of the circulation and to understand the relative contribution of each forcing on the seasonal and yearly mean circulation of the Black Sea. We thus pose similar fundamental questions to those raised in our previous work but now focused to investigate the seasonal variability [*Oguz et al.*, 1995]: (1) what is the relative importance of the wind stress, air-sea thermohaline fluxes, and the lateral buoyancy fluxes in driving the general circulation on the monthly and seasonal timescales; (2) how is the regional variability of these forcing agents related to the spatial variability of the general circulation; (3) how is the circulation modulated by the mesoscale variability generated by the currents in response to the internal dynamical processes; and, finally, (4) is the general circulation dominated by the yearly forcing or by the seasonal cycle?

Section 2 provides a brief outline of the numerical model implementation to the Black Sea configuration. Section 3 presents various features of the climatological surface fluxes and the wind stress fields to aid interpretation of the monthly circulation fields. Section 4 describes results of the numerical experiments. It is followed by a summary and conclusions in section 5.

2. Model Description

The model used in this study is the Princeton Ocean Model (POM) described by *Mellor* [1991]. It is a three-dimensional, f plane, free surface primitive equation model for an incompressible, Boussinesq, and hydrostatic fluid employing the bottom-following sigma coordinate and coast-following orthogonal curvilinear coordinate systems. It includes the Mellor-Yamada level 2.5 turbulence closure scheme [*Mellor and Yamada*, 1982] for the parameterization of vertical mix-

ing. The prognostic equations are those for the horizontal velocity components, temperature and salinity, turbulence kinetic energy, and turbulence macroscale. These turbulence quantities together with the vertical velocity shear and buoyancy are used to determine the vertical mixing coefficients for momentum and thermodynamic variables. The details of model formulation, turbulence closure parameterization, and a study of the model sensitivity to σ coordinate over steep topography are given by *Oguz et al.* [1995] and will not be repeated here.

The model resolves the vertical stratification using 18 vertical levels on the sigma coordinate system. The sigma levels are compressed toward the free surface for a better resolution of the shallow upper layer of about 150 m. Then, the upper 200 m of water column within deepest sections of the sea (~ 2000 m) are represented by nine vertical levels. The vertical discretization used is the one given in Table 1 of *Oguz et al.* [1995]. The model geometry of the basin retains major features of the coastline and the bottom topography. The shallowest depths in the NWS are set to 50 m in the model. The horizontal variability in the bottom topography and mesoscale processes are resolved by typical grid spacing of the order of 10 km, which is 2–3 times smaller than the baroclinic radius of deformation. We note that this spacing reduces to about 5 km along most of the Turkish and Caucasian coast where the steepest topographic slopes are and the rim current has the form of a narrow coastal jet. The model configuration and topography used are shown in Figure 1.

The model is initialized with a horizontally uniform, one-dimensional stratification obtained by basin-wide averaging of the winter climatological data. These profiles are similar to their annual mean counterparts used by *Oguz et al.* [1995]. The main difference occurs only within the upper 35 m due to presence of a cold winter mixed layer of 7°C, instead of the seasonal thermocline shown in Figure 6 of *Oguz et al.* [1995].

3. Properties of Surface Forcings

In the numerical experiments described in the next section the wind stress fields are derived from the monthly mean *Hellermann and Rosenstein* [1983] climatology provided by 1×1 degree resolution. The monthly climatological heat flux Q_H as well as the evaporation E minus precipitation P rate distributions are provided by E. Stanev of the University of Sofia. The monthly heat flux climatology data given by *Efimov and Timofeev* [1990] are similar to that of *Stanev* [1990], since both data sets are constructed from similar data sources. The monthly temperature and salinity fields are based on the climatological atlas prepared by *Altman et al.* [1987]. These data were made available to us on a 60×40 min grid resolution by I. Gertman.

3.1. Monthly Wind Stress Fields

The basin-averaged climatological monthly mean wind speed data set given by *Efimov and Timofeev* [1990] indicates typical wind speeds of 5 m/s during the summer period, increasing to 8 m/s during the winter months (Figure 2). The wind speeds vary linearly between these two extreme values during the spring and autumn seasons. Taking the drag coefficient as 0.0013, the corresponding basin-averaged wind stress values lie in the range from 0.3 to 0.8 dyn/cm² within the year. We found this range to be consistent with the long-term data obtained from several meteorological stations along the Turk-

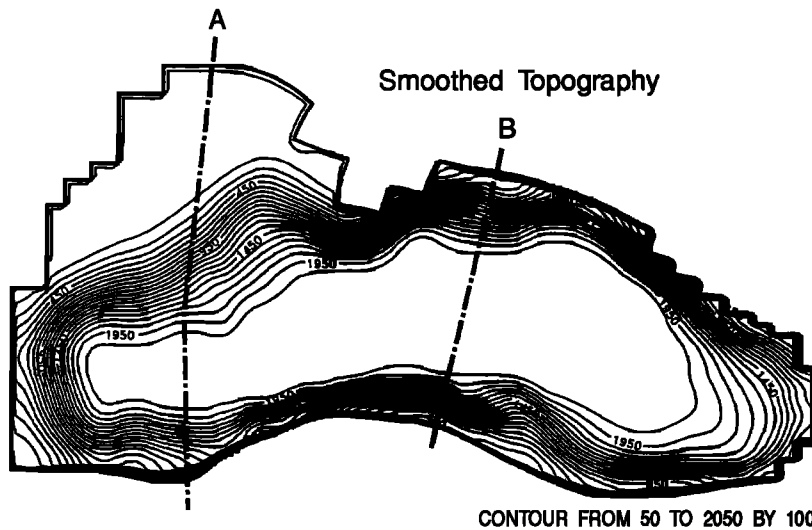


Figure 1. The model configuration and bottom topography (depths are in meters).

ish coast of the Black Sea. The data given by *Hay et al.* [1990] from a Turkish coastal weather station between April 1982 and March 1985 indicate even higher wind stress values: greater than 1.0 dyn/cm² during November–March period with a maximum of 1.5 dyn/cm² in February and of the order of 0.5 dyn/cm² during summer.

When compared with these values, the *Hellermann and Rosenstein* [1983] (HR) wind stress climatology appears to be consistently weaker by a factor of 2–3 throughout the year. HR monthly wind fields give the strongest winds of 0.4–0.5 dyn/cm² during winter and 0.2–0.3 dyn/cm² during summer, the basin average values being approximately half of these maximum values. Although we recognize the weakness of the HR winds, we use this data set because it is the best documented one presently available for this region, agreeing with the others in the directional patterns. Also, we used the HR winds in the previous work of *Oguz et al.* [1995], and we want to compare the yearly circulation and its climatological seasonal cycle driven by the same wind stress forcing.

The month by month analyses of wind stress distributions indicate that the wind stress pattern is almost unchanged throughout the year (see Figure 5 of *Oguz et al.* [1995] for the annual mean pattern). The monthly distributions are all dominated by the northerlies in the western basin, veering cyclonically toward the eastern basin where they become northwest-erlies. Northeasterly winds usually prevail in the southern part of the western basin. The winds tend to be stronger in the western part and weaken toward the eastern end of the sea.

3.2. Monthly Heat Flux Distributions

The basin-averaged monthly climatological net heat flux Q_H variations together with the net radiative flux R_n (defined by the sum of shortwave incoming radiation and longwave back radiation) and the sum of latent heat Q_l and sensible heat Q_s fluxes are shown in Figure 3a. The net heat flux is defined by $Q_H = R_n + (Q_l + Q_s)$ where the fluxes are positive downward from air to sea. Figure 3a shows a cooling trend from the beginning of September to the end of February with greatest cooling rates of ~150 W/m² occurring in December and January. The March–August period corresponds to the warming cycle of the heat flux which attains the maximum value of ~150 W/m² during June. Averaging over the whole year the heat loss and gain approximately balance; the sea gains a net heat from the atmosphere of only ~0.4 W/m². This is compensated by the advective heat loss through the Bosphorus junction.

The most distinguishing feature of the monthly net heat flux patterns in the cooling season (October–February) is the presence of considerable spatial variability within the basin. All the heat flux distributions in the autumn–winter periods show high spatial variability with an almost zonal distribution from the northwestern to southeastern part, as clear in the January pattern of Figure 3b, upper panel. The maximum cooling takes place in the northwestern shelf (NWS) area, and the minimum occurs on the opposite side, near the southeastern end of the basin. These two regions of extreme heat fluxes are separated by a west-east oriented belt of pronounced Q_H variability. The

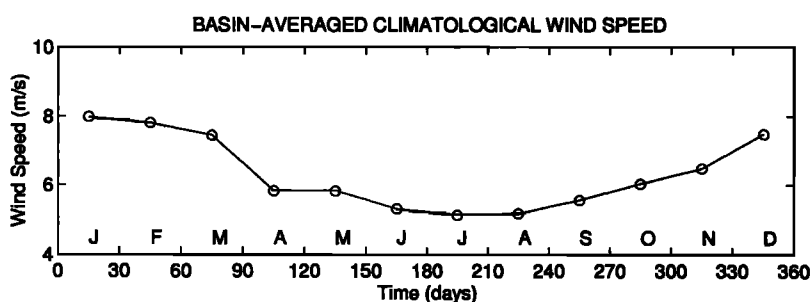


Figure 2. The basin-averaged climatological monthly mean wind speed variations during the year.

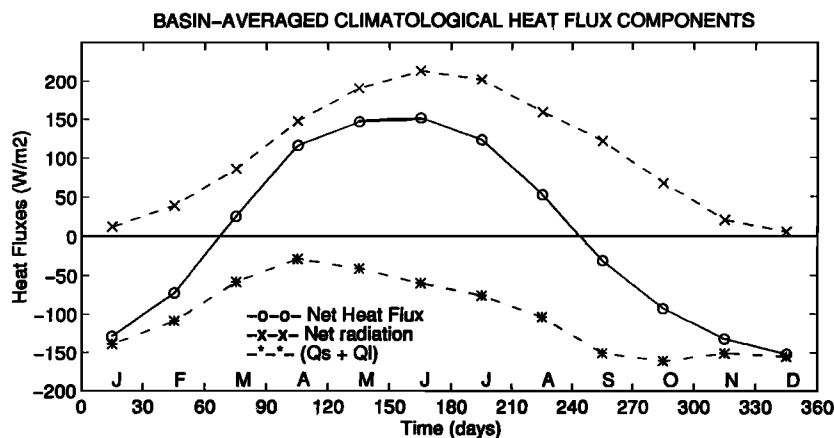


Figure 3a. The basin-averaged climatological monthly variations of the net heat flux (continuous line with open circles), the net radiative flux (crosses), and the sum of latent and sensible heat fluxes (stars) during the year. The data are taken from *Efimov and Timofeev* [1990] and are similar to those obtained by *Stanev* [1990].

strong cooling region of the NWS often extends toward the Turkish coast. The entire western basin is then characterized by stronger cooling rates than the eastern basin. The maximum and minimum cooling rates are about 175 W/m^2 and 100 W/m^2 in December for the western and eastern parts, respectively. The surface cooling tends to decrease afterward to 100 W/m^2 in the western basin and 40 W/m^2 in the eastern basin during February.

April is characterized by a uniformly distributed warming of approximately 75 W/m^2 throughout the basin. It is followed by rapid warming in May, increasing to more than 110 W/m^2 all over the basin with a maximum of 150 W/m^2 in the NWS area. The maximum warming rate takes place in June–July, decreasing slightly in August. As in the winter period the summer Q_H distributions are also characterized by a general pattern. This involves a region of stronger warming covering the basin interior surrounded by relatively weaker warming rates around the periphery, as clear in the July pattern of Figure 3b, lower panel. The onshore-offshore variability in the warming rates is more pronounced along the western coast and near the southeastern end of the basin. The climatological data therefore suggest substantial changes not only in the sign of the heat flux from cooling in winter to warming in summer season but also in their spatial patterns.

3.3. Monthly ($E - P$) Distributions

According to the climatological data given by *Efimov and Timofeev* [1990], the mean evaporation minus precipitation ($E - P$) rate over the basin is 0.37 m/yr (or 31 mm/month). The excess of evaporation is balanced by the fresh water input from the major rivers around the periphery as well as across the Bosphorus Strait. Figure 4a displays the annual variations of evaporation and precipitation rates as well as their difference, positive values representing the excess of evaporation. During December and January the monthly evaporation and precipitation rates almost balance each other. The precipitation exceeds the evaporation rate by about 15 mm/month during the next three months. Evaporation begins to dominate after May, increasing linearly toward a maximum value of $\sim 150 \text{ mm/month}$ in August with the corresponding maximum net ($E - P$) rate of $\sim 110 \text{ mm/month}$.

A permanent feature of the ($E - P$) fields throughout the year is the change from maximum positive values in the NWS

area to maximum negative values in the southeastern extremity. Therefore the NWS region and the northern part of the western basin are always dominated by the excess of evaporation, whereas the reverse situation persists generally in the eastern basin, particularly near the southeastern part of the sea. As expected this spatial structure has a strong seasonal signal. During winter, almost the entire eastern basin as well as the southern parts of the western and central basins are characterized by negative ($E - P$) values, the maximum value being about 100 mm/day (Figure 4b, upper panel). The maximum positive ($E - P$) values in the northwestern region do not exceed 50 mm/day . This situation persists until May. Then, precipitation weakens. The typical summer ($E - P$) distribution exhibits a zone of maximum positive values near the northwestern shelf and in the northern part of the central basin, decreasing toward the southern and eastern coasts. In the easternmost region a narrow but very intense precipitative zone persists (Figure 4b, lower panel). In July the maximum value of ($E - P$) is about 60 mm/day , increasing to 100 mm/day in September and to 125 mm/day in October where the largest ($E - P$) values are found. Evaporation begins to weaken by November and December, as the precipitation starts controlling again the seasonal cycle.

3.4. Monthly Surface Temperature and Salinity Fields

The monthly climatological surface salinity distributions do not differ much from the annual mean distribution in the basin interior. In Figure 5a we show the July surface salinity pattern as a representative example. The main characteristic feature of the monthly salinity climatology is the presence of pronounced variations along the western coast associated with the freshwater discharges from the Danube, Dniepr, and Dniester Rivers. In proximity of the discharges the lateral salinity variations are of the order of about 5 parts per thousand (ppt), decreasing to about $0.5\text{--}1.0 \text{ ppt}$ further south along the Bulgarian coast and around the Bosphorus Strait. A similar but slightly weaker lateral salinity gradient is also present along the southeastern end of the basin, extending northwestward along the Caucasian coast in the direction of the rim current. This gradient is associated with the dilution of the coastal waters by discharge from the River Rioni as well as continuous precipitation in the region throughout the year (Figure 4b). The rest of the basin

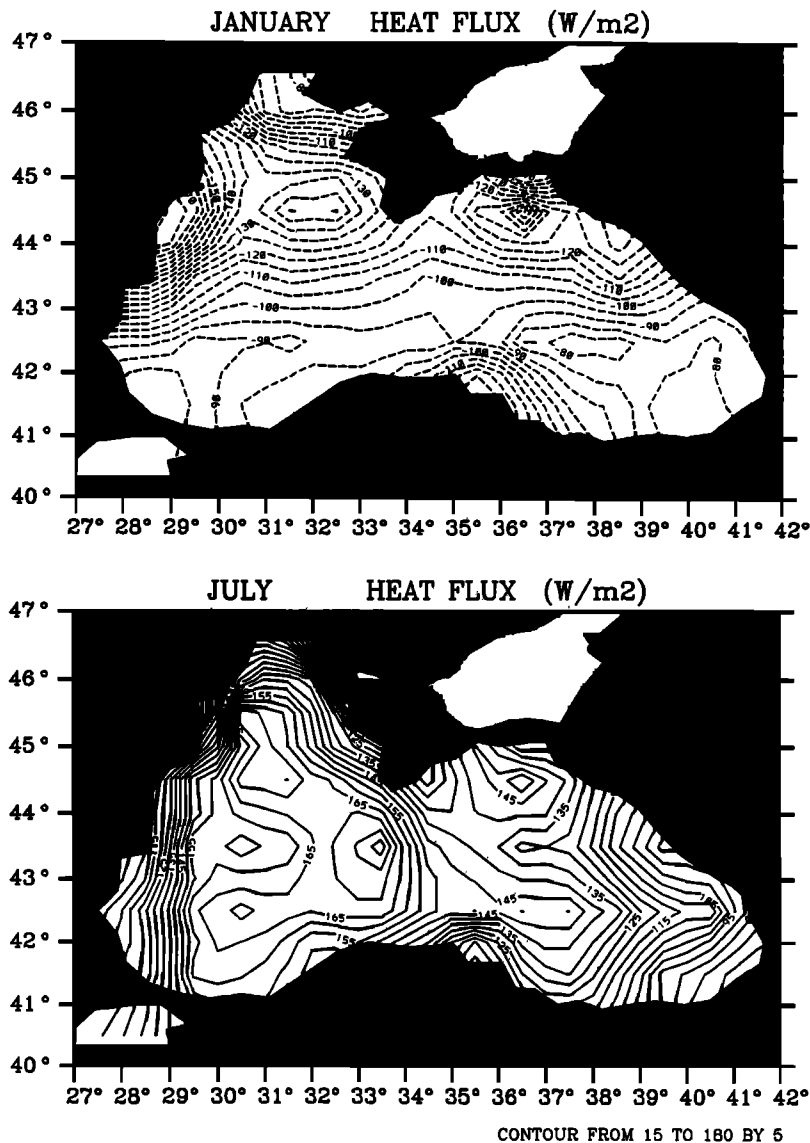


Figure 3b. The climatological net heat flux distributions for the months of (top) January and (bottom) July. The data used are given by *Stanev* [1990].

shows more uniform salinity distributions where the salinity varies typically between 18.1 and 18.4 ppt. These features of the surface salinity distribution are presented in Figure 5a for July. As implied by the recent basin-wide 20×20 min resolution surveys [cf. *Oguz et al.*, 1994], the rim current flow along the Turkish and the northern coasts is accompanied by narrow frontal zones with typical width of 50 km and salinity gradients of less than about 0.5 ppt.

Unlike the salinity fields the horizontal temperature fields exhibit a more pronounced seasonal variability. It is possible to identify two major temperature distributions characterizing the typical summer and winter patterns. The winter distribution represented by the month of February in Figure 5b, upper panel, shows an overall zonal variation. The shallow NWS region, which receives the greatest rate of cooling, is characterized by minimum temperature values of the order of 3°C along the shallowest parts, increasing to 7°C within the outer shelf. The cold water mass formed over the shelf extends further south as a narrow meridional front of cold but fresh water.

The rest of the western and the central basins have a more uniform temperature distribution. The major part of the eastern basin, on the other hand, has a zonal temperature variability with gradual increase toward the end of the basin. As compared with the relatively low winter temperatures in the NWS, the minimum temperatures of the interior are 7.4°C in February and 7.2°C in March. These characteristic values are, however, considerably higher than those observed in the more recent winter cruises where the dense water mass as cold as 5°C was formed within the cyclonic gyres of the interior basin [*Ovchinnikov and Popov*, 1987].

The summer surface temperature distribution represented by the month of July in Figure 5b, lower panel, differs from the winter one in the spatial structure of the interior basin. The relatively lower temperatures in the NWS and higher temperatures within the eastern basin persist also in the summer season. The interior, however, is not as spatially uniform as observed in the winter months, but it shows a zonal temperature gradient of $22^{\circ}\text{--}25^{\circ}\text{C}$ during the July–August period.

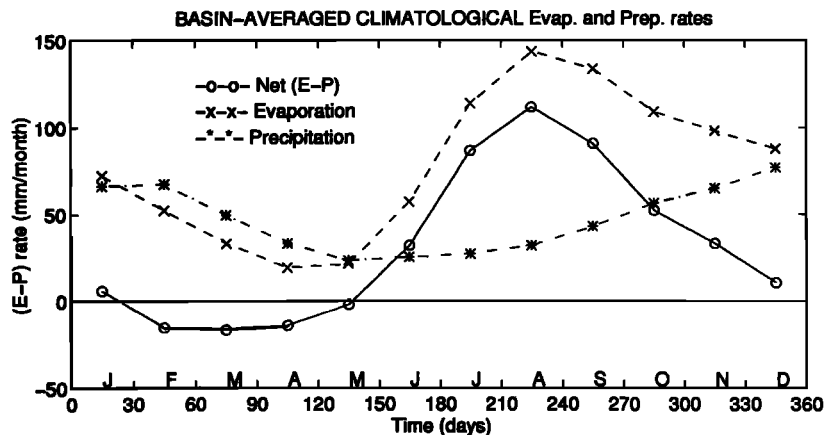


Figure 4a. The basin-averaged climatological monthly variations of the net evaporation minus precipitation ($E - P$) rate (continuous line with open circles), the evaporation rate (crosses), and the precipitation rate (stars) during the year. The data are taken from *Efimov and Timofeev* [1990] and are similar to those obtained by *Stanev* [1990].

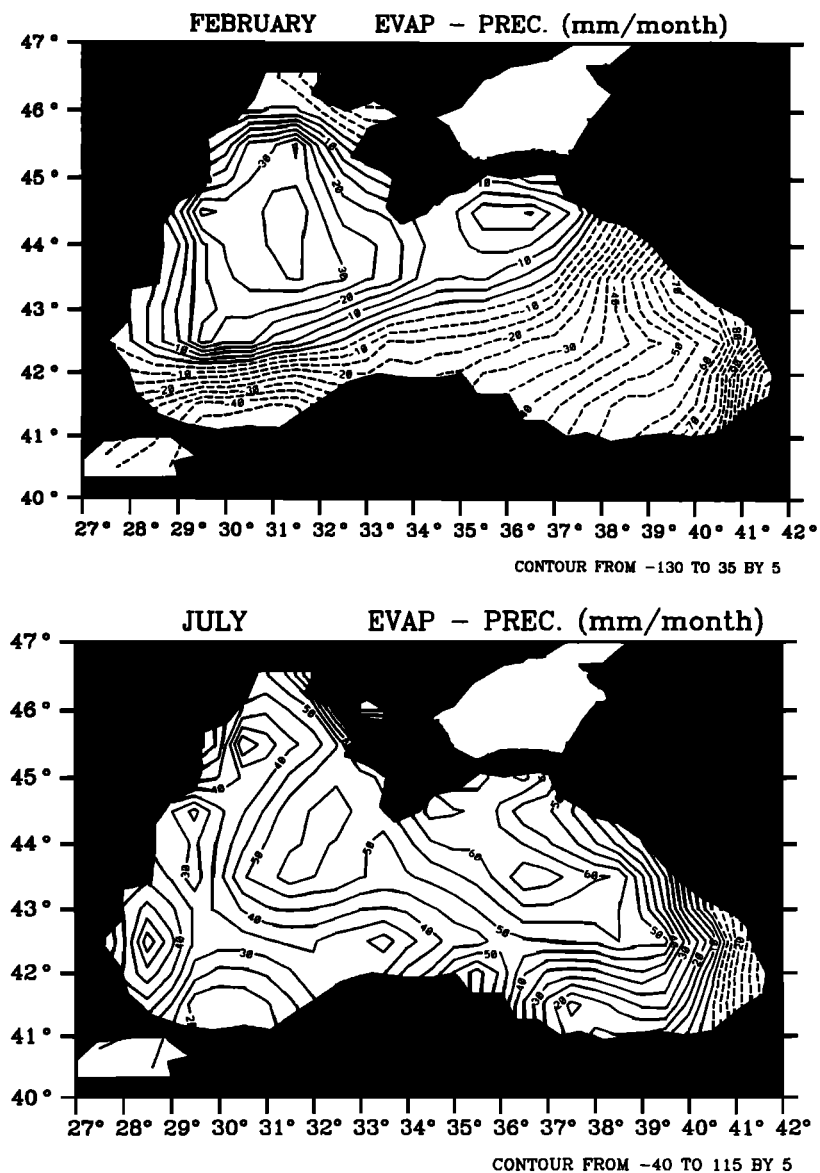


Figure 4b. The climatological net evaporation minus precipitation rate distributions for the months of (top) February and (bottom) July. The data used are given by *Stanev* [1990].

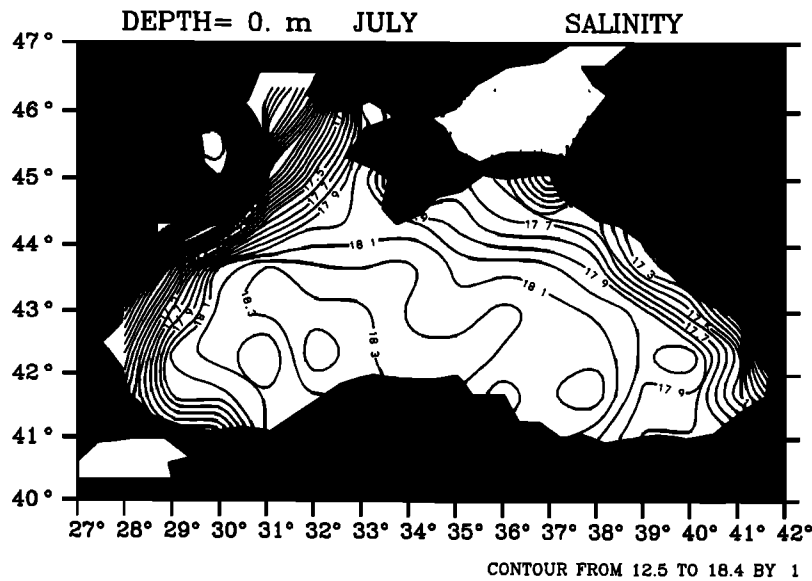


Figure 5a. The climatological surface salinity distribution for July. The data used are given by Altman *et al.* [1987].

4. Numerical Experiments

A total of six numerical experiments listed in Table 1 were carried out to investigate the circulation and water mass characteristics generated in response to different types of forcings during the year. The first experiment considers the wind-driven circulation alone within a “perpetual” year with the seasonal climatological cycle. No surface or lateral buoyancy fluxes are therefore imposed in this experiment. In the second experiment (EXP2A) the response of the system to the horizontally uniform annual cycle of heat flux $Q_H(t)$ of Figure 3a is investigated. The salt flux is not imposed as the surface boundary condition, but the surface salinity $S_s(t)$ is restored to its horizontally uniform yearly cycle with a time constant of 10 days. This experiment is designed to understand the role of the simplest possible surface thermohaline forcing in the development of a convectively generated mixed layer in winter and its subsequent evolution during the rest of the year. These two experiments are carried out in a closed basin configuration in which the curvilinear grid is slightly different from that shown in Figure 1 in the treatment of coastal geometry near the northwestern corner of the basin. Specifically, the grid used in these experiments is the one shown in Figure 3 of Oguz *et al.* [1995]. The third experiment (EXP2B) is a repetition of the second one but using the spatially varying monthly climatological net heat and salt fluxes. In the absence of wind forcing and river runoff this experiment therefore explores the role of spatial variability of the surface fluxes ($Q_H(\eta, \xi, t)$ and $F_s(\eta, \xi, t)$) on the upper layer circulation and water mass characteristics within the year. EXP3A investigates relative contributions of the lateral buoyancy and surface flux forcings on the circulation, especially in the NWS region and during the periods of cold intermediate layer (CIL) formation and spreading phases. EXP3B is similar to EXP3A except the surface thermohaline fluxes are set to half of their original values. EXP4 describes the seasonal circulations driven by all the three major driving mechanisms.

In experiments EXP3A, EXP3B, and EXP4 a uniform freshwater discharge of $10,000 \text{ m}^3/\text{s}$ is prescribed throughout the year near the northwestern corner of the model basin at two

grid points approximating roughly the entrance of the Danube estuary. The temperature and salinity of the inflow are given as $T = 13^\circ\text{C}$ and $S = 5 \text{ ppt}$, as given by Oguz *et al.* [1995]. This temporally uniform specification of the freshwater discharge is used for simplicity and does not affect the circulation and water mass characteristics of the basin in general and of the NWS in particular, since the heat flux forcing adjusts the temperature of the discharge area to its seasonal cycle. The Bosphorus Strait is then opened to compensate heat and salt excesses or deficits in the basin. The entrance is defined by two grid points opening, across which the Mediterranean underflow with $T = 12^\circ\text{C}$ and $S = 23 \text{ ppt}$ is allowed to enter into the basin during the inflow conditions. In these latter experiments the curvilinear grid used is the one shown in Figure 1 that achieves a smoother representation of the coastal geometry near the Danube delta. As noted by Oguz *et al.* [1995], this configuration avoids small-scale noise in the current field developed by interaction of the coastal flow with the stair-step corners.

Time integrations are started from an initial state of rest under “perpetual” year forcing(s) and continued until the climatological seasonal cycle repeats itself. The time evolution of the solution is tracked by monitoring daily values of basin-averaged kinetic energy and of the upper 200-m layer mean temperature and salinity. The spin-up timescale is of the order of 3 years, and the equilibrium state for the upper layer circulation is usually reached in the fourth and fifth years. Clearly, attainment of the equilibrium state for the deep thermohaline circulation is much longer and requires an order of magnitude longer integration period. In the present work, our major goal is to study the seasonal upper layer circulation characteristics in response to different combinations of driving mechanisms. The model results presented here are thus based on the fifth year’s time integration using daily mean fields to filter high-frequency variability.

4.1. Circulation Driven by Wind Stress Alone

The yearly evolution of the upper layer circulation fields generated in response to the HR wind stress climatology is described in this section. Figures 6a–6d show monthly mean

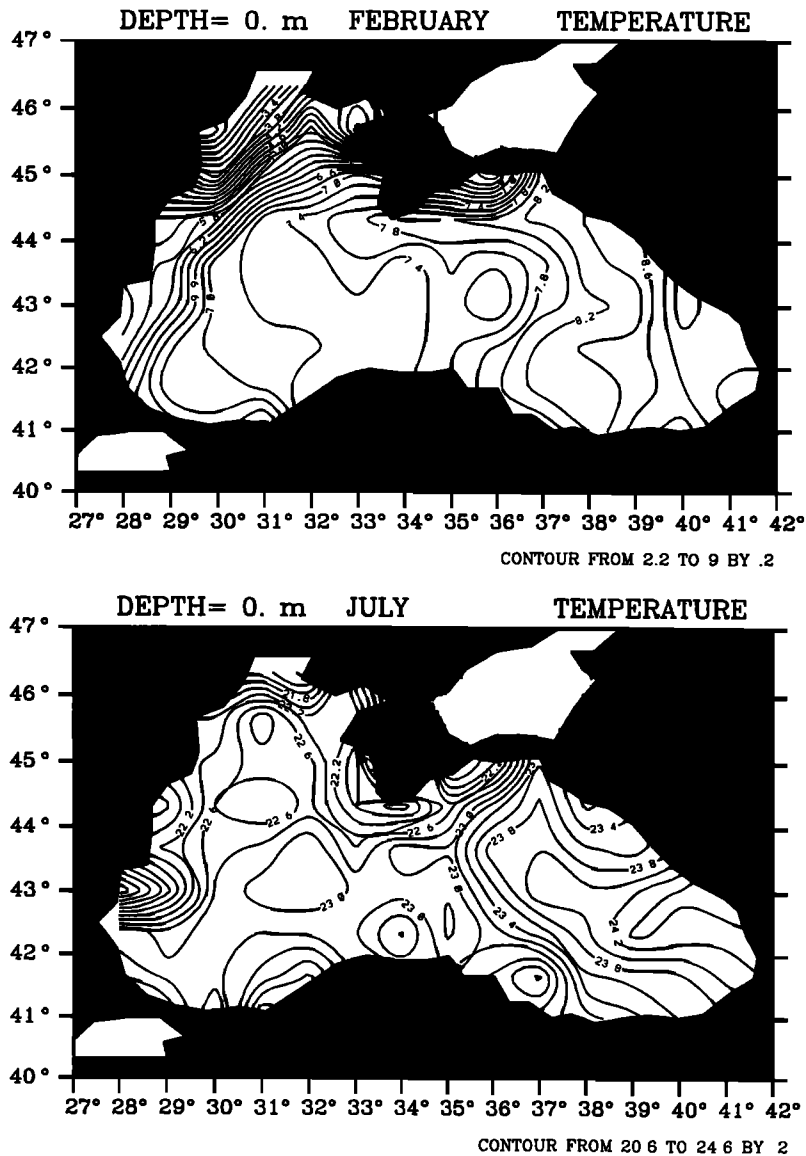


Figure 5b. The climatological surface temperature distribution for the months of (top) February and (bottom) July. The data used are given by Altman et al. [1987].

surface (5 m) circulation patterns for February, May, August, and November, taken as representative for the four seasons. The main characteristic features of these patterns are evident subs basin scale gyres and mesoscale variability with pronounced evolution of the flow field. The main, permanent feature of the upper layer circulation that persists all year long is a well-

defined cyclonic boundary current system around the periphery of the basin. Two other robust features are the anticyclonic gyre in the NWS and the strong cyclone in the southwestern end, off the Bosphorus. The near-coastal part of the boundary current system always follows the steep continental slope and is characterized by small-amplitude meanders that do not seem to grow to finite amplitude. The rim current is broader along the northern coastline as well as the shelf break continental slope between the NWS and the basin interior. The offshore part of the NWS anticyclone lies on the shelf break and forms a major part of the boundary current system near the western coast. In the February pattern (Figure 6a) the inner part of the central and eastern basins is occupied by an elongated cyclonic cell. It has a well-defined peripheral current system with two cyclonic gyres of the order of 100 km in size. Meandering of the rim current offshore the Turkish and Crimean coasts decouples the western basin circulation from the rest of the interior circulation. The coastal anticyclonic eddies along the western coast and to the west of the Crimean peninsula have been

Table 1. List of Numerical Experiments

Experiment No.	Wind Stress Forcing	Lateral Buoyancy Forcing	Forcing for Temperature Equation	Forcing for Salinity Equation
1	on	off	off	off
2A	off	off	$Q_H(t)$	$S_s(t)$
2B	off	off	$Q_H(\eta, \xi, t)$	$F_s(\eta, \xi, t)$
3A	off	on	$Q_H(\eta, \xi, t)$	$F_s(\eta, \xi, t)$
3B	off	on	$\frac{1}{2}Q_H(\eta, \xi, t)$	$\frac{1}{2}F_s(\eta, \xi, t)$
4	on	on	$\frac{1}{2}Q_H(\eta, \xi, t)$	$\frac{1}{2}F_s(\eta, \xi, t)$

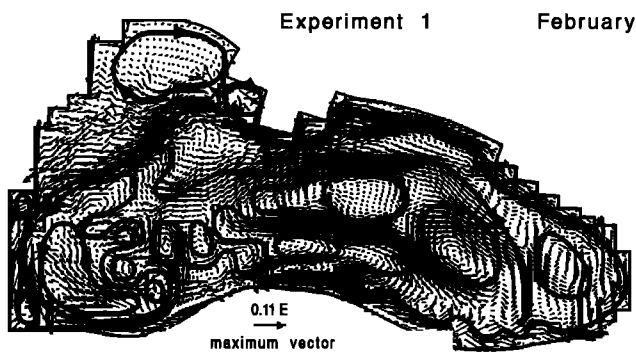


Figure 6a. The 5-m wind-driven circulation pattern for February. Maximum currents are scaled by 10 cm/s for clarity of presentation of the circulation. A schematic diagram of the circulation features is also included on the figure.

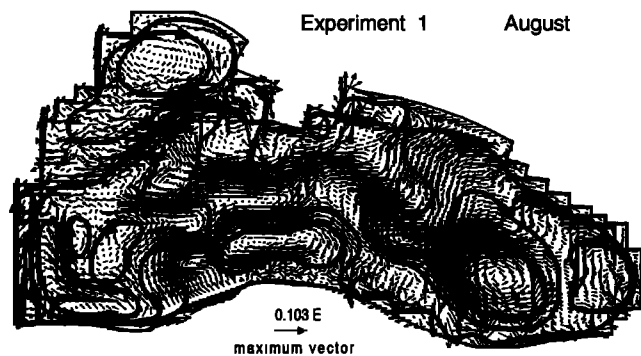


Figure 6c. The 5-m wind-driven circulation pattern for August. Maximum currents are scaled by 10 cm/s for clarity of presentation of the circulation. A schematic diagram of the circulation features is also included on the figure.

identified as quasi-persistent features of the circulation system from the hydrographic observations [Oguz *et al.*, 1993].

The May circulation pattern (Figure 6b) reveals further evolution of the meandering rim current system with intense mesoscale activity. Both the near-shore and offshore components of the rim current exhibit a more pronounced variability along the northern coast, which makes the interior cyclonic cell narrower, formed by four interconnected cyclonic structures. This picture of circulation is further changed by amplification of the meanders along the northern coast during August (Figure 6c). Two major meanders are now observed along the Caucasian coastline. Two oppositely flowing currents are present in the interior of the basin, without any cyclonic interior cell. The only feature of the interior cell left from the May circulation is the circular, strong cyclonic eddy of the eastern basin. The large amplitude meander (or an offshore jet) that penetrates almost 200 km offshore from the Caucasian coast in the southeastern direction is similar both in shape and location to the one observed in the September 1991 survey that persisted for a few months (August–October) as noted in satellite imageries [Oguz *et al.*, 1994]. The November pattern (Figure 6d) shows pinching off from the offshore jet extending southwestward from the northern coast of a small offshore anticyclonic-cyclonic eddy pair. A broad westward flow is found between these offshore features and the coast. In the southern part the interior anticyclone of the central basin is grown further in size.

This experiment shows that the only feature of the upper layer circulation persisting all year long is the basin-wide cyclonic boundary current system. Some permanent structures are present such as the anticyclone in the NWS and the cyclonic gyre near the southwestern corner. Otherwise, the seasonal cycle of the wind stress forcing induces a continuous time evolution of the interior subbasin cells plus a ubiquitous, intense, and highly variable mesoscale activity.

4.2. Circulation Driven by Surface Fluxes

4.2.1. Horizontally uniform heat flux forcing alone. In the absence of any other forcing the horizontally uniform annual heat flux cycle used in EXP2A is not able to generate sufficiently strong baroclinic pressure gradients to drive an appreciable circulation. This experiment is, however, instructive to understand some basic features of the thermohaline structure of the upper layer during different seasons of the year. The uniform heat flux forcing gives rise to a relatively uniform temperature and salinity fields within the basin interior but generates considerable cross-shore gradients around the periphery that are locked to the strong topographic changes. The interior waters in winter are always cooler and denser than those around the periphery. In February the typical monthly mean surface water temperature is 6°C in the interior, increasing to a maximum value of 9°C near the coast and in the NWS (Figure 7a).

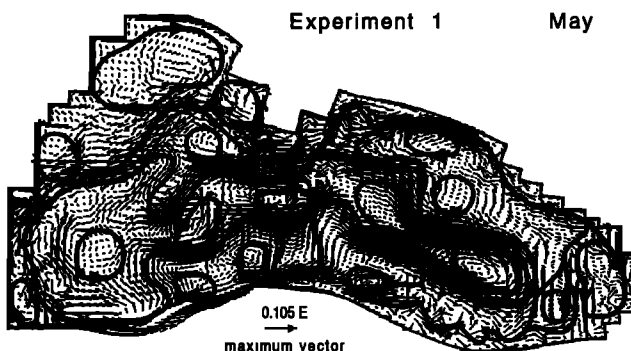


Figure 6b. The 5-m wind-driven circulation pattern for May. Maximum currents are scaled by 10 cm/s for clarity of presentation of the circulation. A schematic diagram of the circulation features is also included on the figure.

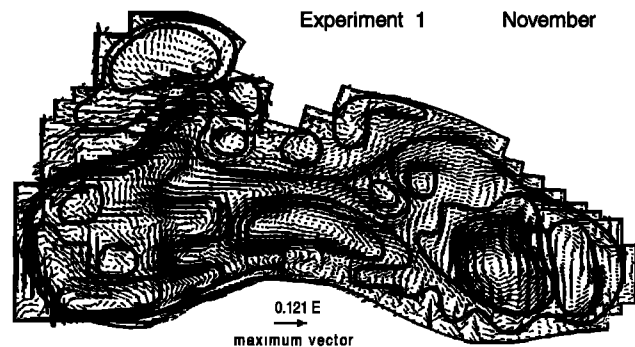


Figure 6d. The 5-m wind-driven circulation pattern for November. Maximum currents are scaled by 10 cm/s for clarity of presentation of the circulation. A schematic diagram of the circulation features is also included on the figure.

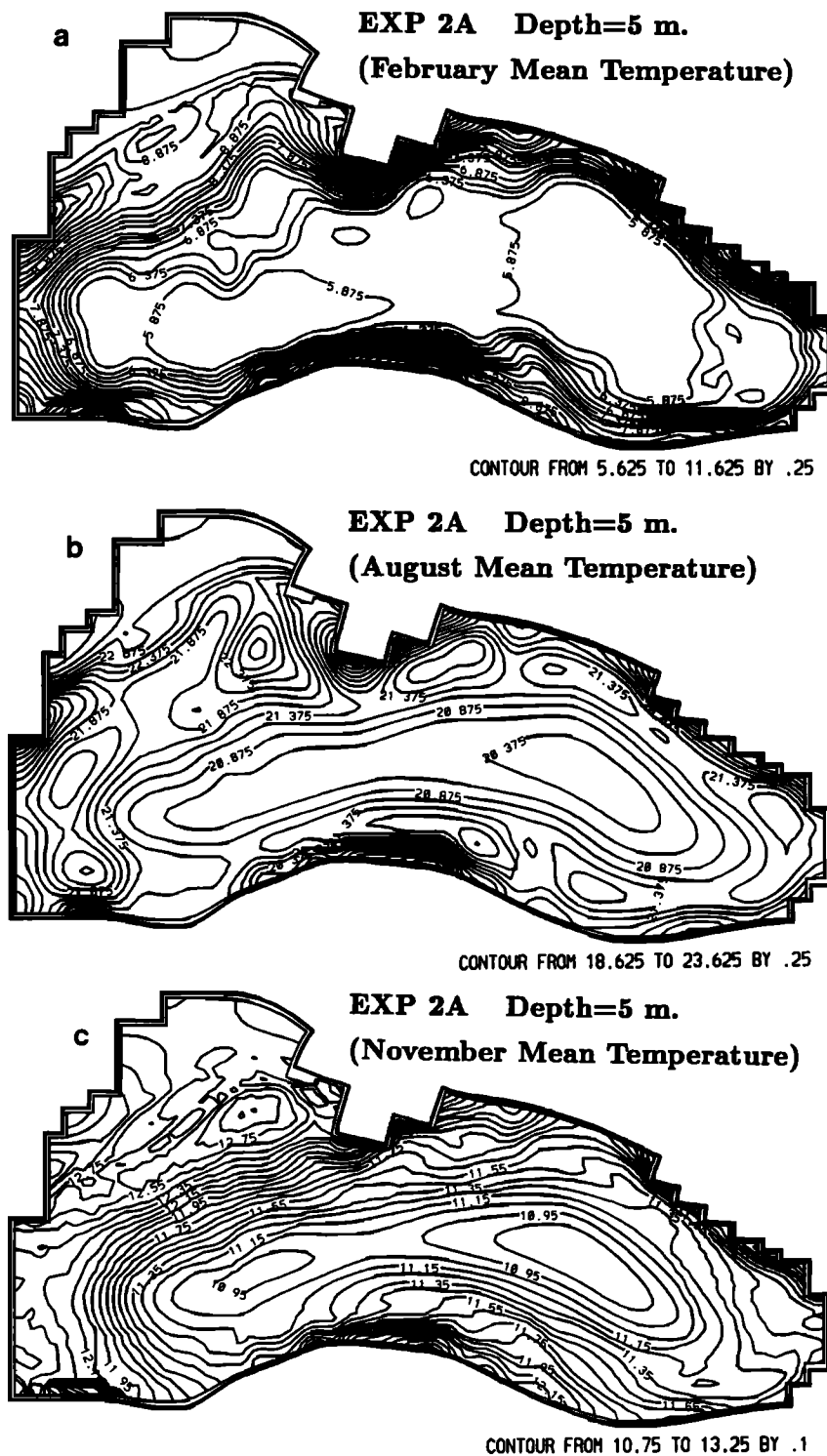


Figure 7. The 5-m monthly mean temperature (degrees Celsius) distributions for (a) February, (b) August, and (c) November for the circulation driven by the horizontally uniform heat flux cycle only (EXP2A).

As the surface waters become warmer in spring, the on-shore-offshore temperature differences are reduced gradually, and the temperature structure starts developing mesoscale features around the periphery. The mesoscale activity begins to intensify in June, as the meanders grow and give birth to mesoscale detached eddies, leaving a narrow zone of colder waters close to the Turkish and Caucasian coasts (Figure 7b).

In summer the shallow NWS region stores the maximum heat in the basin and consequently attains the highest temperature, exceeding those of the central basin by more than 2°C. The successive wintertime cooling cannot make these warmer waters cooler than the interior waters. In November the transition period occurs when the interior waters start to cool and become cooler than the coastal waters (Figure 7c). The summer

mesoscale activity dies off gradually, and the system reverts back to its more coherent, spatially uniform structure observed in winter.

As a further illustration of the change of the interior water mass structure due to the seasonality of the surface thermal fluxes, we show the vertical sections of temperature and density along the north-south transect across the center of the basin marked as "section B" in Figure 1. The temperature and density vertical distributions during February (Figure 8a) illustrate the vertical extent of the newly formed cold water mass with temperature and density values of about 6.0°C and 14.6 kg/m³, respectively, in the mixed layer that occupies the basin interior.

After the convection event ceases and surface waters begin to warm by surface heating during the following spring, the seasonal thermocline begins to develop, and the core of the CIW remains sandwiched between the relatively warmer waters of the seasonal and permanent thermoclines (Figure 8b). The winter to summer temperature contrast observed in the peripheral waters has been noted previously in the climatological temperature data as well as in satellite imagery [Oguz *et al.*, 1992]. The seasonal reversal of the coastal-deep water temperature gradients has been interpreted as a consequence of the upwelling events caused by prevailing northeasterly winds [Oguz *et al.*, 1992]. The upwelling is certainly a process which may contribute to development of such temperature gradients. This experiment, however, suggests that the winter-to-summer changes of the thermal fluxes by themselves may induce such reversal of the coastal-offshore temperature gradients within the year.

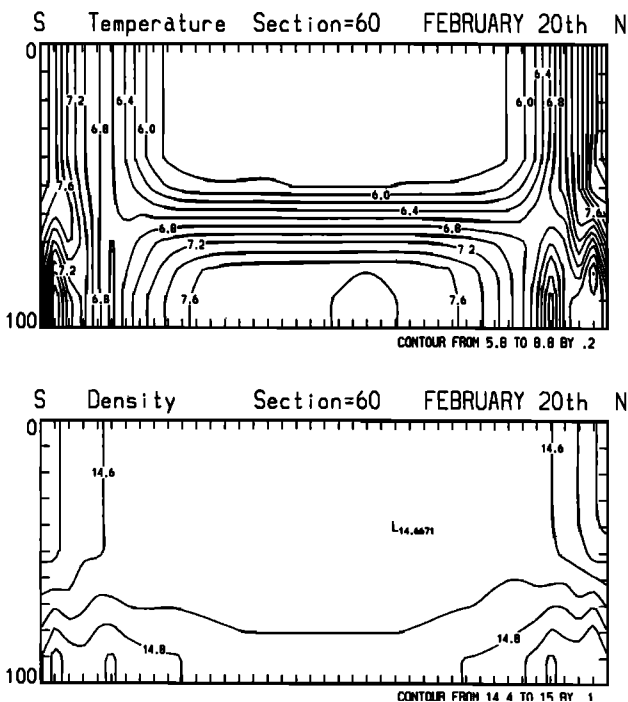


Figure 8a. The monthly mean February (top) temperature (degrees Celsius) and (bottom) density (kilograms per cubic meter) vertical distributions for the upper 100 m across section B for the circulation driven by the horizontally uniform heat flux cycle only (EXP2A). The position of section B is marked in Figure 1.

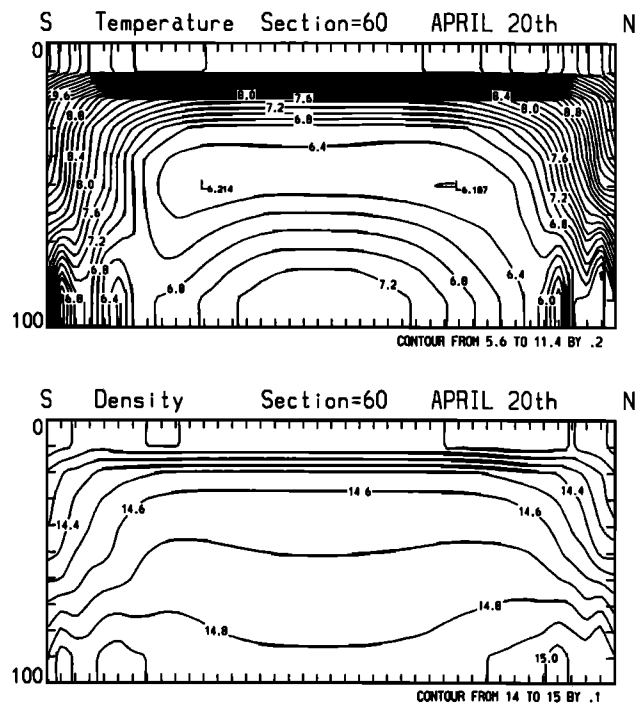


Figure 8b. The monthly mean April (top) temperature (degrees Celsius) and (bottom) density (kilograms per cubic meter) vertical distributions for the upper 100 m across Section B for the circulation driven by the horizontally uniform heat flux cycle only (EXP2A). The position of section B is marked in Figure 1.

4.2.2. Horizontally varying surface flux forcing alone.

The previous experiment is repeated in EXP2B with the horizontally changing climatological monthly heat and salt flux forcings to explore how the circulation and water mass characteristics are sensitive to spatial variability of the surface fluxes. A major contribution of the heat and salt flux horizontal variabilities is to develop a circulation field which is comparable in strength to the wind-driven case with typical surface currents of about 15 cm/s. The upper layer circulation field reflects essentially structures of the heat and (*E - P*) fields. The winter circulation is characterized by two zonally elongated basin-wide cells (Figure 9a). The southern cell is anticyclonic and is driven by the excess of precipitation over evaporation (see Figure 4b) whose effect dominates the relatively weaker heat flux contribution in the southern basin. The northern cell is instead cyclonic and driven by the relatively stronger cooling present in the northern part. This structure provides an eastward zonal flow within the interior, westward currents along the southern and northern coasts. The northwestern shelf circulation is governed by a cyclonic gyre which is an extension of the northern basin circulation.

The basin has considerable temperature differences from the northwestern shelf to the southeastern region. The northern part is cooler with the lowest surface temperatures of about 2°C in the NWS. The temperatures increase in the offshore direction to about 7°C within the central part of the western Black Sea and to about 10°C within the southeastern eddy.

The summer circulation and temperature fields (Figure 9b) are also correlated with the corresponding heat flux distribution characterized by stronger warming within the interior basin and weakening toward the periphery. Thus the temperature

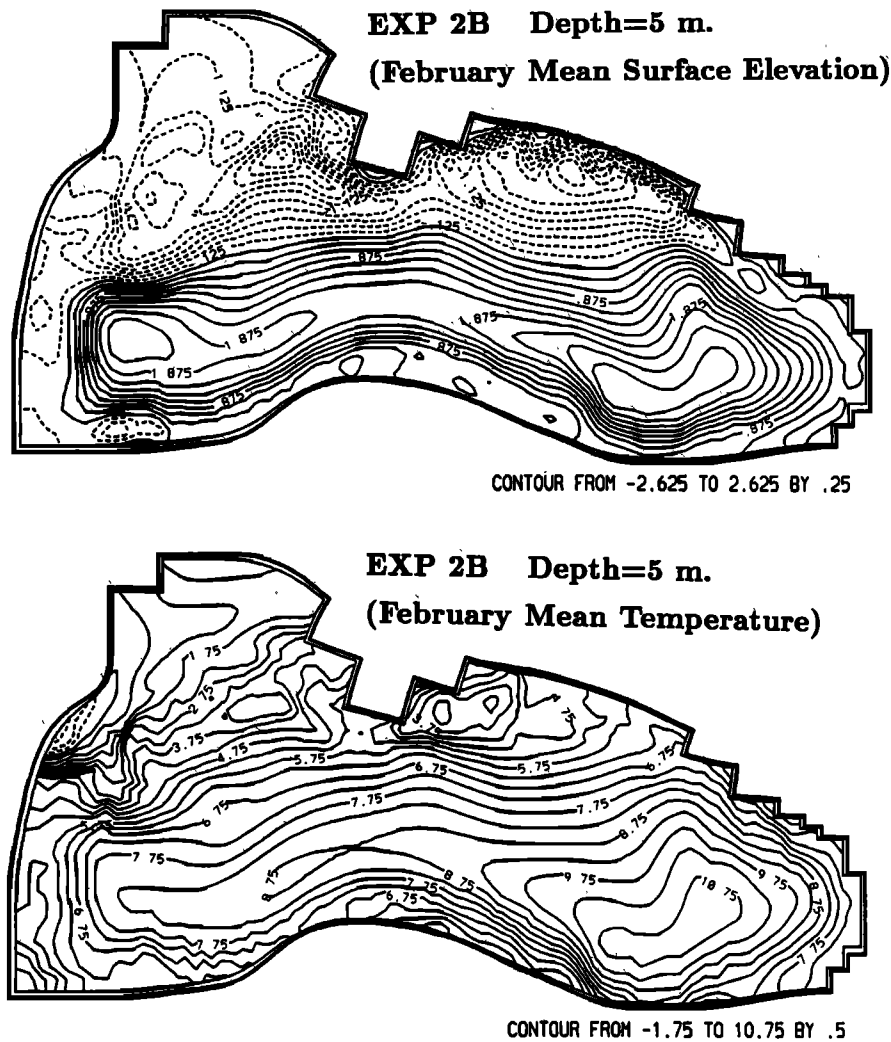


Figure 9a. The 5-m monthly mean February (top) surface elevation (centimeters) and (bottom) temperature (degrees Celsius) distributions for the circulation driven by the horizontally varying surface fluxes only (EXP2B).

field is warmer and relatively uniform inside the basin but possesses stronger variability where the cooler and denser coastal waters are present. The resulting density field generates a basin-wide anticyclonic circulation with more pronounced meandering along the periphery than that observed in the previous experiment. Again, the temperature field possesses diagonal variability. When compared with the climatological surface temperature distributions of Figure 5b, the model gives consistently much cooler temperatures in the NWS and warmer ones near the southeastern part during the year. This suggests that the heat flux climatology used in the model provides too strong cooling in the NWS during winter and too strong warming in the eastern basin during summer.

4.3. Circulation Driven by Surface Fluxes and Freshwater Discharge

The experiment EXP3A we describe first in this section is designed to explore how the additional contribution of the lateral buoyancy forcing due to the freshwater discharge into the NWS region modifies the circulation driven by the surface fluxes. As demonstrated by *Oguz et al.* [1995], the freshwater discharge alone is capable of driving a basin-wide cyclonic

circulation around the periphery, together with an anticyclonic gyre occupying the entire NWS [*Oguz et al.*, 1995, Figures 13a–13c]. As shown in Figures 10a and 10b the major effect of the lateral buoyancy forcing is to replace the NWS wintertime cyclonic gyre of the previous experiment with a stronger anticyclone throughout the year. In the winter months a smaller cyclonic cell remains decoupled from the NWS, which occupies only the central basin interior. This cell breaks the overall anticyclonic cell into two subbasin scale anticyclonic gyres situated in the western and eastern basins. The winter circulation (Figure 10a, upper panel) thus comprises two anticyclonic and one cyclonic gyres in the interior plus the NWS anticyclone. The major effect of the freshwater discharge is seen on the temperature structure of the upper layer (Figure 10a, lower panel). Once the anticyclonic gyre is formed and decouples the NWS from the rest of the basin, the strong cooling (of the order of 150 W/m^2 for about 3 months) on this shallow (about 50 m) water body gives rise to extremely low water temperatures, as low as -5°C . These unrealistic, cold shelf waters are separated from those of the western basin by a very strong temperature front at the shelf break.

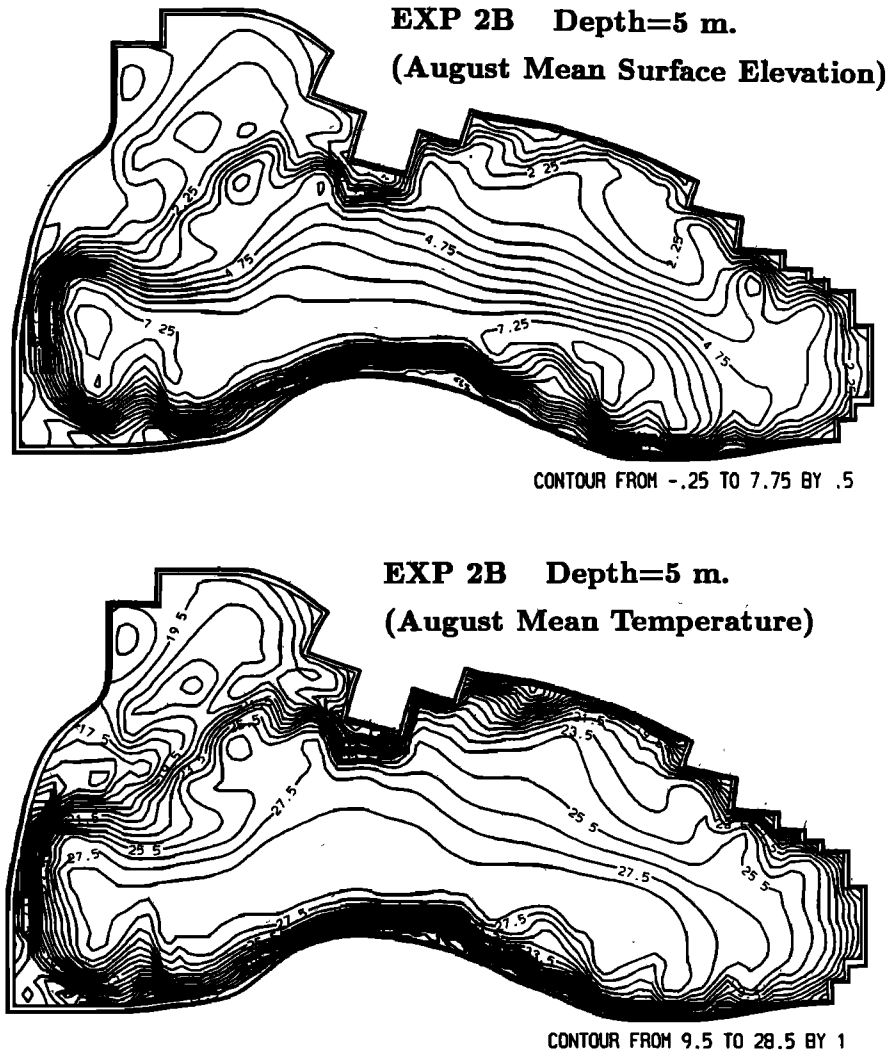


Figure 9b. The 5-m monthly mean August (top) surface elevation (centimeters) and (bottom) temperature (degrees Celsius) distributions for the circulation driven by the horizontally varying surface fluxes only (EXP2B).

The main features of the winter circulation persist also in the summer months (Figure 10b). The cyclonic gyre of the central basin disappears, and an overall anticyclonic circulation is induced by the surface heating. The surface temperature has even more unrealistically large zonal variability, ranging from 13°C in the NWS to 29°C near the eastern corner of the basin.

This experiment demonstrates clearly that the monthly climatological surface fluxes in general and the heat flux in particular impose too strong a cooling on the NWS during winter months and too strong a warming in the eastern basin during the summer months. The resulting water mass characteristics of the upper layer are substantially different from the observations throughout the year.

The experiment EXP3A is repeated reducing by half the intensity of the heat and salt surface fluxes. The goal is to have an estimate of fluxes capable of generating a more realistic thermohaline structure in the different regions of the basins during the year. The surface elevation patterns and 5-m depth temperature distributions for February and August are shown in Figures 11a and 11b. As expected the circulation patterns (Figures 11a and 11b, upper panels) are very similar to those of

EXP3A except for the weakening of the anticyclonic circulations and the intensification of the cyclonic gyre of the central basin which is now present all year long. The anticyclonic gyre of the eastern basin is now much weaker, demonstrating how strongly the precipitation controls the circulation in this region. Compared with the climatological surface temperature distributions shown in Figure 5b, the winter surface temperatures (Figure 11a, lower panel) reveal a more realistic horizontal distribution varying from 2°C in the NWS to 8°C in the eastern basin. The surface temperatures of 5°–6°C within the interior of the basin are also typical for the winter period. The summer surface temperatures (Figure 11b, lower panel), however, vary between 10°C and 17°C and are much cooler than the observed values. The summer surface temperature changes generated by halving the surface fluxes in the eastern basin are therefore drastic and about 10°C. This experiment suggests that half of the value of the original fluxes may be a reasonable estimate for the winter season, whereas a smaller reduction of the heat flux intensity should be sufficient for the summer season. The major implication of these experiments is the crucial need for a thorough reanalysis of the monthly heat and salt flux clima-

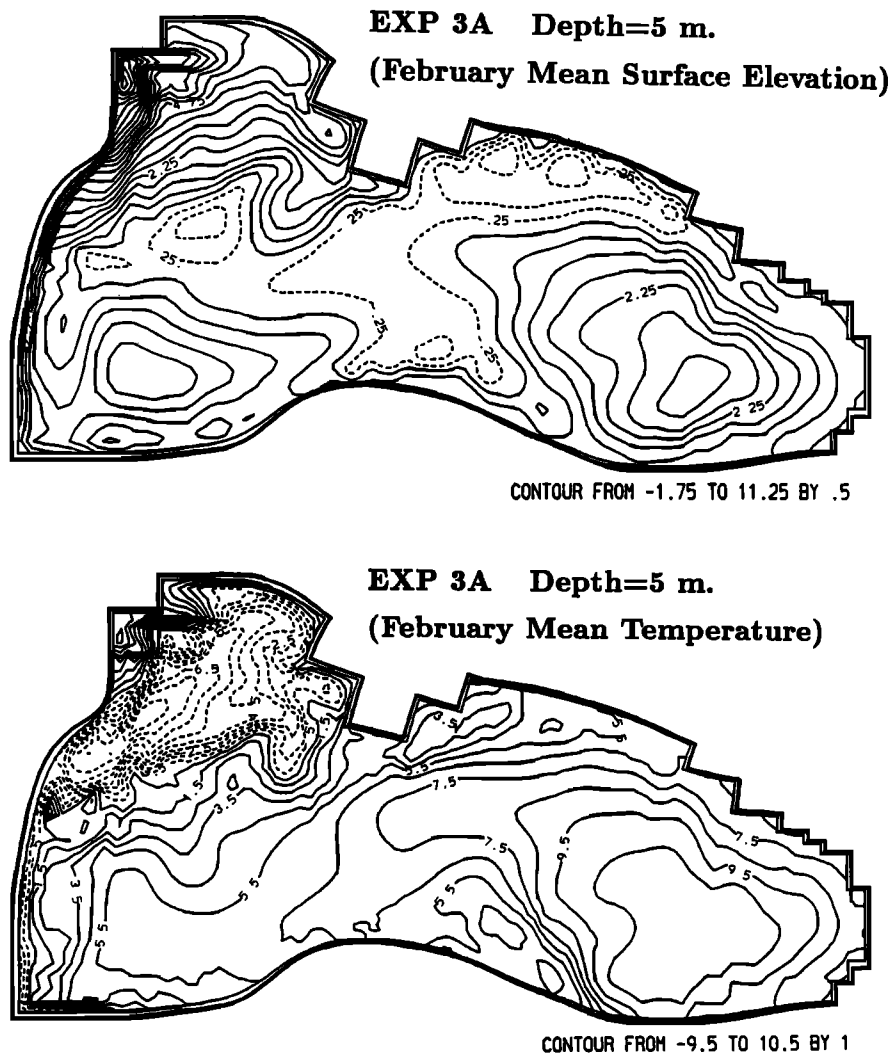


Figure 10a. The 5-m monthly mean February (top) surface elevation (centimeters) and (bottom) temperature (degrees Celsius) distributions for the circulation driven by the combination of the horizontally varying surface fluxes and the lateral river discharge forcings (EXP3A).

tologies. This reanalysis is of absolute priority for the success of future modeling efforts leading to fully realistic simulations of the general circulation and water mass characteristics in the Black Sea.

4.4. Circulation Driven by Wind Stress, Surface Fluxes, and Freshwater Discharge

The surface circulations at 5-m depth driven by the combination of all forcings are shown for February, May, August, and November in Figures 12a–12d. The circulation patterns exhibit a combination of the dominant features of these three independent forcings, such as the anticyclonic gyre over the NWS, the cyclonic gyre of the southwestern basin, the peripheral current system along the steep continental slope all around the basin, and its small-amplitude meandering due to the jet internal dynamics. Most of the small-scale gyre variability introduced by the wind forcing is smeared out by the larger-scale structures of the thermohaline-driven circulation. The main features of the February (winter) circulation (Figure 12a) are the cyclonic cell covering the central and southern part of the eastern basin, whereas the northern part is occupied by the anticyclonic gyre elongated along the Caucasian coast. The

winter general circulation therefore shows an almost equal contributions of cyclonic and anticyclonic cells and exhibits much more structural variability than the basin-wide cyclonic coherent cell proposed earlier [see Tolmazin, 1985, Figure 35].

The winter circulation modifies gradually in the spring period. As shown by the May circulation in Figure 12b, the anticyclonic gyre of the southwestern basin is shifted eastward and merges with the boundary current system. The anticyclonic gyre of the eastern basin has grown in size and penetrates further south. The main features of the spring circulation resemble the overall winter pattern, showing only gradual shifts of structures in position and intensity.

The summer circulation shown in Figure 12c is, on the other side, very different from the winter and spring ones. One main difference is the disappearance of the anticyclonic gyre of the eastern basin, which leads to a large cyclonic cell covering the entire eastern and central basins. We recall that the source of the anticyclonic gyre is the strong precipitation during the winter and spring months. As in summer the precipitation weakens considerably and concentrates to a narrow zone along the eastern end of the basin (Figure 4b), the anticyclonic gyre

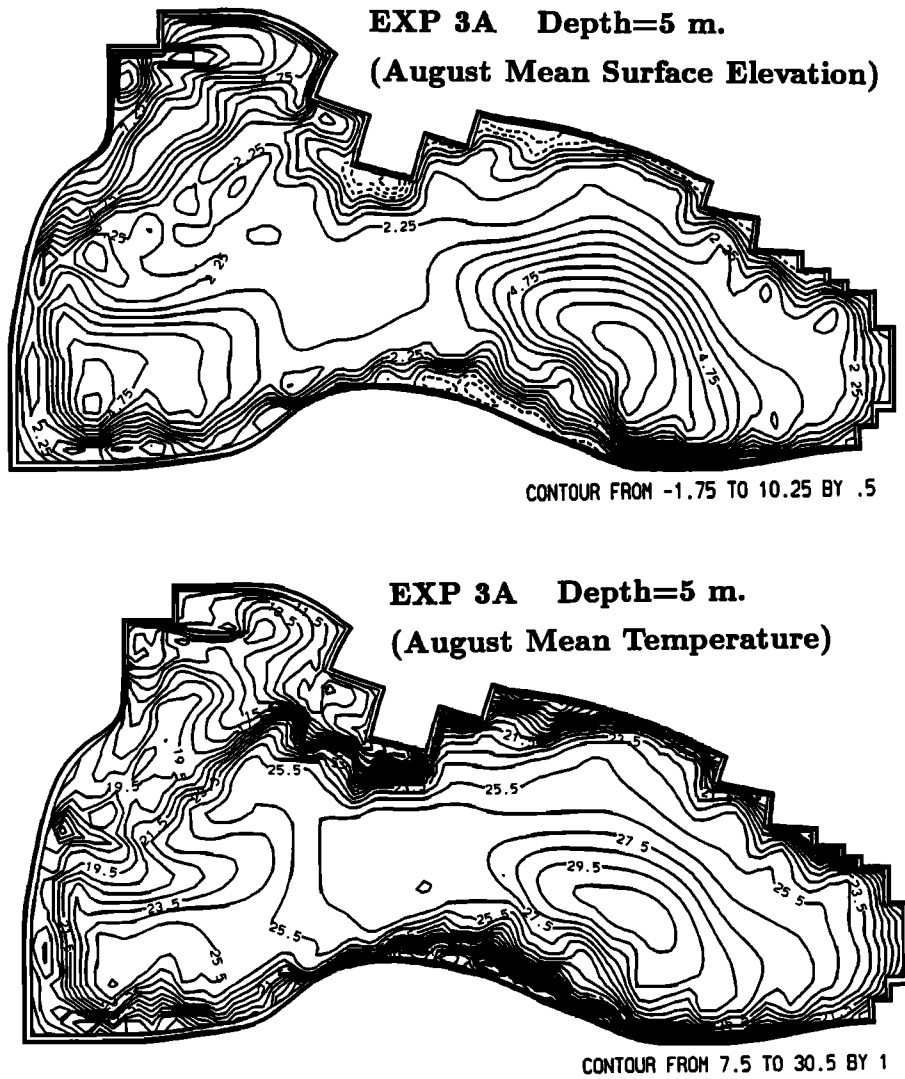


Figure 10b. The 5-m monthly mean August (top) surface elevation (centimeters) and (bottom) temperature (degrees Celsius) distributions for the circulation driven by the combination of the horizontally varying surface fluxes and the lateral river discharge forcings (EXP3A).

is confined near the eastern coast and becomes a coastally trapped eddy. The southern anticyclone in the western basin is translated slightly further east, and its zonal extent is reduced by almost half. The westernmost basin is occupied by a larger-scale cyclonic gyre.

The November surface circulation (Figure 12d) exhibits further evolution of the summer pattern showing a gradual return to winter distribution of Figure 12a. Thus the location and sizes of all major subbasin gyres are intermediate between the winter and summer configuration.

We finally display in Figures 13a and 13b the water mass characteristics of the upper 100 m of the water column shown as section A in Figure 1. This section is oriented approximately in north-south direction extending from the NWS to the vicinity of the southern coast. The mid-February vertical distribution of the temperature and density (Figure 13a) shows the convectively generated cold water masses with temperatures of about 4°–6°C extending to depths of 50–75 m. In the NWS as well as more south in the center of the western basin, the previously formed mixed layer is stratified by the horizontal circulation. The only region which shows an entirely homoge-

nized mixed layer down to ~75 m is the anticyclone close to the southern coast of the western basin. The temperature and density of this region are characterized by homogeneous values of approximately 5°C and 14.6 kg/m³, consistent with the observations. We note, however, that even though the shelf waters have relatively cooler temperatures, their lower salinity due to the freshwater discharge makes the density considerably lower (>1.0 kg/m³) than the interior values. This density gradient between the shelf and the interior leads to a strong shelf break front during winter which prevents the spreading of the shelf-originated colder waters into the interior by cross-isobath motions. As suggested by the shape of the isopycnals, the mixed layer waters of the interior sink toward the topographic slope where they are advected by the rim current all around the periphery of the basin.

The August vertical distributions of the temperature and density shown in Figure 13b further illustrate how the different characters of the shelf and interior water masses are preserved even 6 months after the CIW formation. Waters with temperatures 5.6°–5.8°C and densities less than 14.2 kg/m³ are trapped within the lowest levels of the shelf by the strong shelf

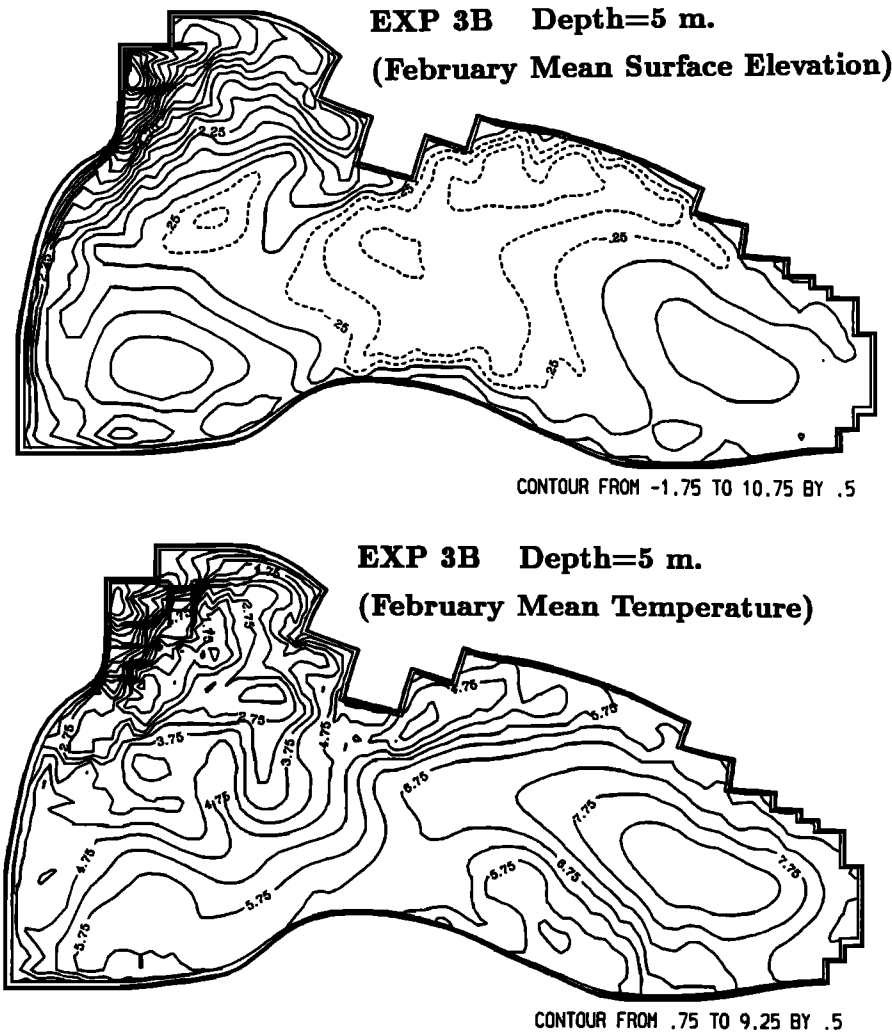


Figure 11a. The 5-m monthly mean February (top) surface elevation (centimeters) and (bottom) temperature (degrees Celsius) distributions for the circulation driven by the combination of the reduced horizontally varying surface fluxes and the lateral river discharge forcings (EXP3B).

break front. A water mass with temperatures of 6.0° – 6.6°C and density varying between 14.2 and 15.0 kg/m^3 is confined within the narrow continental slope region. This is the CIL water mass circulating with the rim current along the periphery of the basin. Below the seasonal thermocline, in the zone of the CIL core, this coastal tongue of cold water is separated from the interior CIL by a density front extending parallel to the continental slope on the offshore side of it. Thus the interior CIL keeps its distinct character identified by about 6.0°C temperature and 14.5 – 14.7 kg/m^3 density values until the next winter formation event breaks the seasonal thermocline and renews the existing CIW.

5. Conclusions

The seasonal variability of the Black Sea circulation is studied in this paper to explore the individual roles of climatological forcings by the wind stress, surface thermal and salt fluxes, and the lateral freshwater discharge. A synthesis is made of the results with those obtained under yearly climatological conditions by *Oguz et al.* [1995] to assess whether the major circulation features are a response to the yearly forcings or are

dominated by the seasonal cycle. The general basin circulation is found to show, under all forcing mechanisms, a strong seasonal cycle that dominates the yearly cycle. Only a few localized gyre structures persist throughout the year. In the purely wind-driven circulation a well-defined boundary current system is established; its near-coastal branch exhibits strong meanders and interactions with the interior flow structures. The interior of the basin undergoes a strong seasonal evolution characterized by subbasin scale cyclonic gyres that interact, split, and coalesce throughout the climatological year. The subbasin scale circulation is further modulated by strong mesoscale activity leading to the formation of cyclonic/anticyclonic eddies along the peripheral current system. This intense mesoscale activity is evidently linked to the meanders and instabilities of the rim current and is reminiscent of the surface patterns observed in satellite imagery.

Contrary to the wind stress forcing, the thermohaline fluxes tend to generate a simpler circulation pattern, but with a comparable strength. In winter the circulation is characterized by a pair of zonally elongated basin-wide cells. The northern cell is cyclonic and induced by the response of stronger cooling,

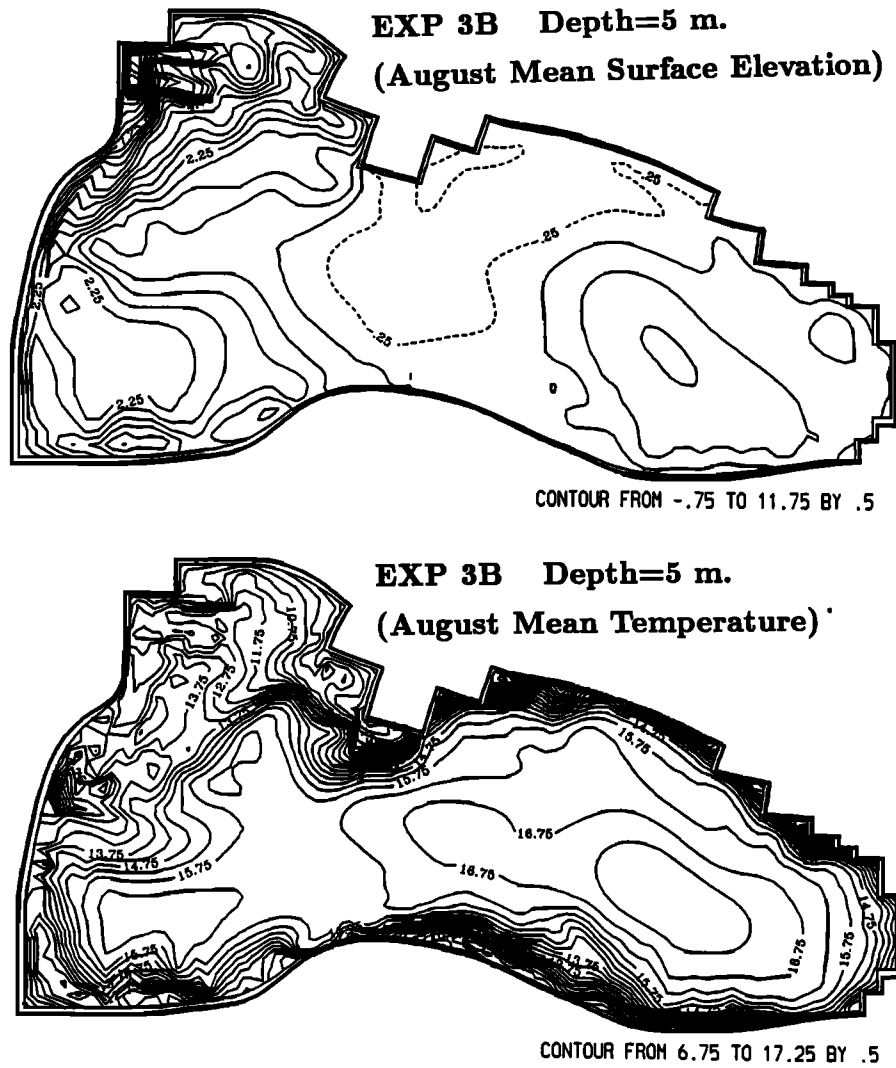


Figure 11b. The 5-m monthly mean August (top) surface elevation (centimeters) and (bottom) temperature (degrees Celsius) distributions for the circulation driven by the combination of the reduced horizontally varying surface fluxes and the lateral river discharge forcings (EXP3B).

whereas the southern cell is anticyclonic and developed by the dominant effect of precipitation. In summer, both warming and excess of evaporation generate a basin-wide anticyclonic cell. Because the thermohaline circulation tends to oppose the

purely wind-driven one for most of the year within the major part of the basin, the strength and richness in the circulation structures seen in the purely wind-driven case are reduced considerably under combined forcings. The mesoscale activity

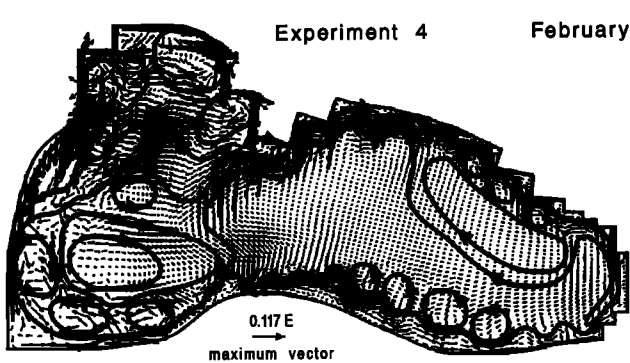


Figure 12a. The 5-m monthly mean February circulation pattern driven by the combination of all forcings (EXP4). A schematic diagram of the circulation features is also included on the figure.

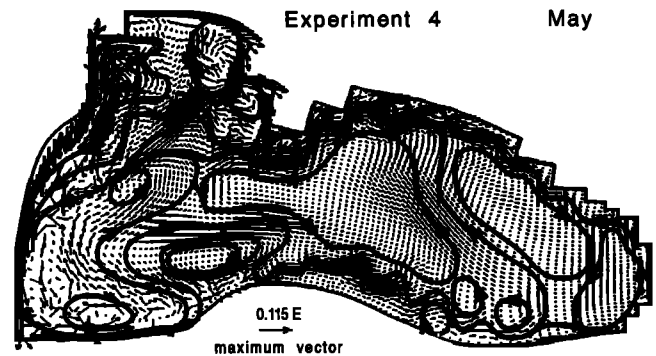


Figure 12b. The 5-m monthly mean May circulation pattern driven by the combination of all forcings (EXP4). A schematic diagram of the circulation features is also included on the figure.

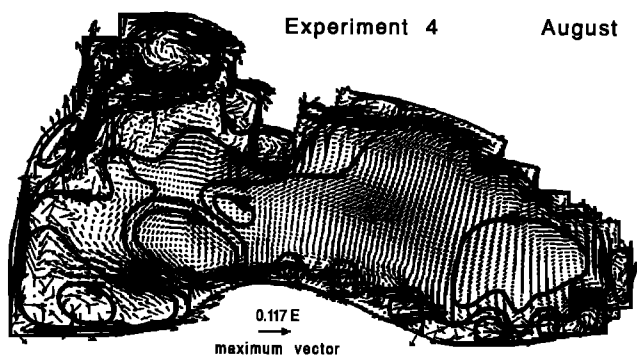


Figure 12c. The 5-m monthly mean August circulation pattern driven by the combination of all forcings (EXP4). A schematic diagram of the circulation features is also included on the figure.

then becomes mostly confined to the peripheral rim current system, linked to its dynamical instabilities.

The simplicity in the interior structure of the circulation driven by all forcings, however, disagrees with the observations [Oguz *et al.*, 1992, 1993, 1994]. In this respect the model experiments have two major implications. First, the circulation produced by the wind stress forcing alone resembles more the observed upper layer circulation patterns. The wind stress forcing thus seems to play a more dominant role in controlling the upper layer circulation in the Black Sea. But, as already discussed by Oguz *et al.* [1995], the Hellermann and Rosenstein [1983] climatology underestimates the wind stress forcing and therefore is unable to drive a sufficiently strong circulation in the basin. A more realistic representation of the Black Sea upper layer circulation would require a stronger wind stress forcing dominating the thermohaline effects that compensate for it in the present simulations. Second, the necessity of re-analysis of heat flux climatology emerges as an important by-product of this work. The existing data seem to impose too strong local coolings and/or warmings which make the water mass characteristics sometimes inconsistent with the available observations. This does not critically alter the overall upper layer circulation features but prevents reasonably realistic horizontal distributions of the surface temperature. Even though the heat flux climatology used is unable to reproduce the annual cycle of the sea surface temperature distributions, the

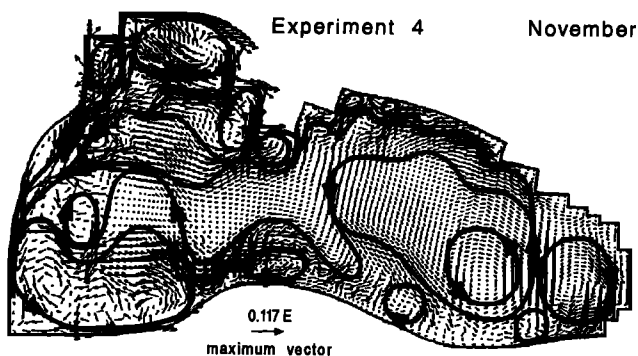


Figure 12d. The 5-m monthly mean November circulation pattern driven by the combination of all forcings (EXP4). A schematic diagram of the circulation features is also included on the figure.

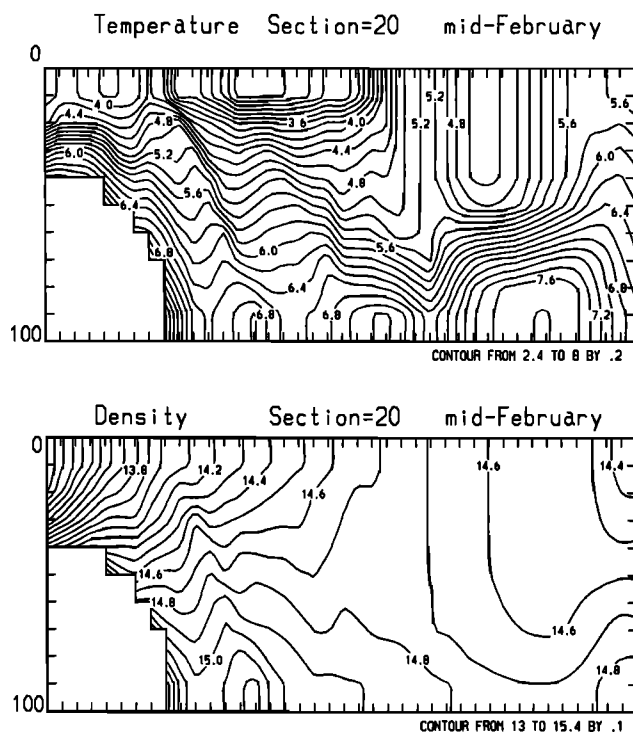


Figure 13a. The mid-February (top) temperature (degrees Celsius) and (bottom) density (kilograms per cubic meter) vertical distributions for the upper 100 m across section A for the circulation driven by the combination of all forcings (EXP4). The position of section A is marked in Figure 1.

wintertime cold water mass formation process is simulated well with the right density ($14.5\text{--}14.8\text{ kg/m}^3$) and thickness (50–75 m) as well as its yearly evolution.

The seasonal circulations reveal a two-layer structure, similar to that obtained by the annual mean forcings of Oguz *et al.* [1995]. The upper layer circulation is almost uniform within the first 100 m. The lower layer circulation appears also to be uniform below 250- to 300-m depths. We however note that, in our limited-period simulations typically 5 years long, the lower layer circulation will not be affected significantly by surface forcings. It mostly reflects the initial conditions used and is very similar to the yearly pattern of Oguz *et al.* [1995, Figure 18b], since the lower layer initial stratifications are the same in both works. The sharp density contrast between the upper and lower layers ($\sim 5\text{--}6\text{ kg/m}^3$ in summer and $\sim 2.5\text{--}3\text{ kg/m}^3$ in winter) acts as an insulator for the downward penetration of the response to the surface forcings. Thus the changes of the thermohaline structure of the lower layer can be investigated only in long-duration simulations (~ 100 years).

A final important finding of the present work is to quantify the secondary role of the NWS in the CIW formation process, as was also previously shown by Stanev [1990]. This is particularly true during high-to-moderate river discharge winters, as in the present simulations. Even though the most intensified cooling and subsequent formation of coldest waters takes place here, the freshwater supply from the River Danube prevents the shelf waters from being dense enough to spread into the deep basin interior by crossing over the topographic slope. They are effectively trapped within the subsurface levels of the NWS for most of the year and only advected gradually in along shelf direction with the local circulation features. During the

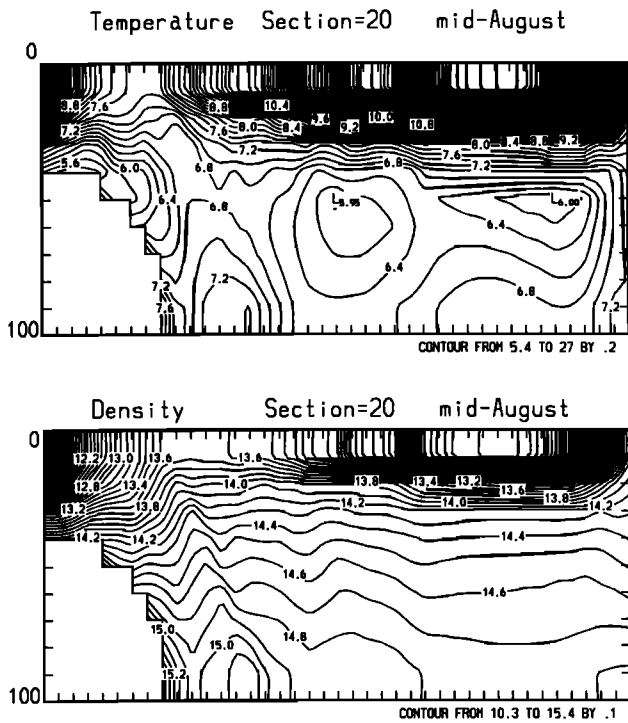


Figure 13b. The mid-August (top) temperature (degrees Celsius) and (bottom) density (kilograms per cubic meter) vertical distributions for the upper 100 m across section A for the circulation driven by the combination of all forcings (EXP4). The position of section A is marked in Figure 1.

weak freshwater winters, however, the NWS may contribute to the overall dense water mass formation with densities comparable with those of the interior.

Acknowledgments. This research was initiated by the NSF grant INT.9310226 when T. Oguz was a visiting scientist at MIT during the June 1993 to July 1994 period. It was later completed with the support of the ONR grant N00014-95-1-0226. Under this grant, T. Oguz was a visiting scientist at MIT during June–August 1995. T. Oguz was also supported partially by the NATO Science for Stability Program TU-Black Sea Project as well as by the Turkish Scientific and Technical Research Council (TUBITAK).

References

Altman, E. N., I. F. Gertman, and Z. A. Golubeva, *Climatological Fields of Salinity and Temperature in the Black Sea*, 109 pp., Sevastopol Branch, State Oceanogr. Inst., Sevastopol, Ukraine, 1987.

Efimov, V. V., and N. A. Timofeev, Investigation of the Black Sea and Azov Sea heat balance, technical report, 237 pp., Ukr. Acad. of Sci., Sevastopol, Ukraine, 1990.

Hay, B. J., S. Honjo, S. Kempe, V. A. Ittekkot, E. T. Degens, T. Konuk, and E. Izdar, Interannual variability in particle flux in the south-western Black Sea, *Deep Sea Res., Part A*, 37, 911–928, 1990.

Hellermann, S., and M. Rosenstein, Normal monthly wind stress over the World Ocean with error estimates, *J. Phys. Oceanogr.*, 13, 1093–1104, 1983.

Mellor, G. L., *User's Guide for a Three Dimensional, Primitive Equation, Numerical Ocean Model. Prog. in Atmos. and Ocean. Sci.* 35 pp., Princeton Univ., Princeton, N. J., 1991.

Mellor, G. L., and T. Yamada, Development of a turbulence closure model for geophysical fluid problems, *Rev. Geophys.*, 20, 851–875, 1982.

Oguz, T., P. E. La Violette, and U. Unluata, The Black Sea circulation: Its variability as inferred from hydrographic and satellite observations, *J. Geophys. Res.*, 97, 12,569–12,584, 1992.

Oguz, T., V. S. Latun, M. A. Latif, V. V. Vladimirov, H. I. Sur, A. A. Markov, E. Ozsoy, B. B. Kotovshchikov, V. V. Eremeev, and U. Unluata, Circulation in the surface and intermediate layers of the Black Sea, *Deep Sea Res., Part I*, 40, 1597–1612, 1993.

Oguz, T., et al., Mesoscale circulation and thermohaline structure of the Black Sea observed during HydroBlack'91, *Deep Sea Res., Part I*, 41, 603–628, 1994.

Oguz, T., P. Malanotte-Rizzoli, and D. G. Aubrey, Wind and thermohaline circulation of the Black Sea driven by yearly mean climatological forcing, *J. Geophys. Res.*, 100, 6845–6863, 1995.

Ovchinnikov, I. M., and Y. I. Popov, Evolution of the cold intermediate layer in the Black Sea, *Oceanology*, Engl. Transl., 27, 555–560, 1987.

Stanev, E. V., On the mechanisms of the Black Sea circulation, *Earth Sci. Rev.*, 28, 285–319, 1990.

Stanev, E. V., V. M. Rousenov, N. H. Rachev, and J. V. Staneva, Sea response to atmospheric variability: Model study for the Black Sea, *J. Mar. Syst.*, 6, 241–267, 1995.

Tolmazin, D., Changing coastal oceanography of the Black Sea, I, Northwestern Shelf, *Prog. Oceanogr.*, 15, 217–276, 1985.

P. Malanotte-Rizzoli, Department of Earth, Atmospheric and Planetary Sciences, Massachusetts Institute of Technology, Room 54-1416, Cambridge, MA 02139. (e-mail: rizzoli@ocean.mit.edu.)

T. Oguz, Institute of Marine Sciences, Middle East Technical University, Erdemli 33731, Icel, Turkey.

(Received October 12, 1995; revised March 5, 1996; accepted March 19, 1996.)